VNU Journal of Science: Natural Sciences and Technology, Vol. 40, No. 3 (2024) 1-12

VNU Journal of Science: Natural Sciences and Technology

Journal homepage: https://js.vnu.edu.vn/NST

Original Article

Characteristics and Methylene Blue Adsorption Capacity of Pyrochar Derived from Lemongrass Residue

Truong Thi Thao[1,*], Vuong Truong Xuan[1], Hoang Manh Hung[2], Nguyen Ngoc An[2], Nguyen Sy Duong[2]

[1]*TNU-University of Sciences, Tan Thinh, Thai Nguyen City, Thai Nguyen, Vietnam*
[2]*Gang Thep High School, Trung Thanh, Thai Nguyen City, Thai Nguyen, Vietnam*

Received 28th May 2024
Revised 20th August 2024; Accepted 21st August 2024

Abstract: In this study, the lemongrass essential oil distillation residue (LR) was the first pyrolyzed under air-controlled conditions at 500 °C for 1 hour (B500), followed by activation through alkali treatment under ultrasonic conditions at 70-80 °C for 3 hours (B5KOH). B5KOH displayed a porous architecture with heightened surface area, 79.90 m^2/g, twice the specific surface of B500 material; and carbon content elevated to 87.99%. The material contained some organic functional groups such as C=O, C=C, and C-O-C. The B5KOH sample exhibited the most effective MB uptake at pH 8, achieving adsorption equilibrium within a brief timeframe of approximately 30 – 50 minutes across a concentration spectrum of MB ranging from 5 to 500 mg/L at material loadings of 1-10 g/L, q_m is 74.44 mg/g. The material demonstrated substantial recyclability, maintaining nearly consistent adsorption efficiency through the fifth cycle (decreasing marginally from 96.69% to 95.13%). Experimental adsorption conformed to the Freundlich isotherm adsorption model and proceeds via a second-order kinetic model. The adsorption phenomenon was spontaneous, primarily driven by physical interactions between the B5KOH and MB molecules. Overall, lemongrass-derived pyrochar exhibited considerable promise as an adsorbent material for mitigating MB pollution.

Keywords: Pyrochar, lemongrass, adsorption, methylene blue.

1. Introduction

The latest statistics recently show that approximately 10^6 tons of synthetic dyes are produced annually [1]. Of which, a large part is methylene blue (MB), a cationic dye, that is widely utilized across textile, leather, paper, pharmaceutical, food, and cosmetic industries [2]. Nonetheless, up to about 25% of textile dyes are lost during production and discharged into the environment [3]. MB exhibits high persistence, reduces the amount of dissolved oxygen in water, and limits the ability of aquatic organisms to adsorb light and bioaccumulate through the food chain. Ingestion of methylene blue-contaminated

* Corresponding author.
E-mail address: thao.tt@tnu.edu.vn

https://doi.org/10.25073/2588-1140/vnunst.5271

water can precipitate adverse effects including cyanosis, tissue necrosis, emesis, shock, and heightened cardiac activity [2]. Research demonstrates the inhibitory effects of MB on growth, pigmentation, and protein levels in algae species such as Chlorella Vulgaris and Spirulina platensis [4], alongside teratogenic impacts on murine and zebrafish models [5]. Notably, an ingestion of 5 mg/kg methylene blue can impede monoamine oxidation, leading to serotonin toxicity and potentially fatal outcomes in humans [6]. Collectively, MB is implicated in various complications affecting digestive, respiratory, central nervous, cardiovascular, reproductive, dermatological, and other physiological systems [7]. Consequently, MB pollution represents a substantial threat to both aquatic ecosystems and human health.

The treatment and removal of residual MB from water have been extensively researched and implemented using various methods including physical methods, chemical methods, and biological methods. Among these, adsorption is a physical method with numerous advantages, including technical simplicity, and high efficiency, which can be further enhanced by selecting appropriate adsorbents [8]. Biochar, both pyrochar and hydrochar, derived from agricultural and industrial by-products, is currently a subject of intensive research, utilizing inexpensive raw materials, and reducing waste and CO_2 emissions into the environment. Moreover, biochar shares many characteristics with activated carbon, showing potential as an adsorbent material for treating various types of pollutants, including both organic and inorganic substances [9]. Hence, numerous biomass types have been studied for the production of biochar to treat various pollutants, particularly for MB adsorption, examples include globe artichoke leaves [10], coconut shell [11], corncob [12], lychee seed [13], seed of Cedrela odorata L [14], oil palm empty fruit branch [15], mint-stalks [16], etc. Lemongrass, extensively cultivated in numerous tropical and subtropical regions, serves diverse purposes, either directly utilized in daily life or processed into essential oils [17], thereby generating a notable volume of lemongrass essential oil distillation by-products (LR). Handling methods for this residue commonly encompass combustion, burial, or integration into soil matrices for agricultural purposes. Despite some exploration into the use of lemongrass biochar for soil enhancement [18], investigations into its production as an adsorbent material remain scant [19], particularly concerning its potential for MB adsorption. The distillation process is already a pre-treatment step, making the LR clean, fibrous, and porous, very convenient for biochar production, time, and temperature pyrolysis will be lower than other biomass. It is also convenient and suitable for large-scale production if needed.

Given the predominant presence of cellulose in lemongrass, as evidenced by chemical structure analyses [20], in this study, we undertook the pyrochar from lemongrass essential oil distillation residue (LR) with incorporated alkali activation, scrutinizing its structural attributes, and assessing its efficacy in MB adsorption from aqueous solutions.

2. Experimental

2.1. Equipment and Chemicals

Chemicals (analytical grade purity): Potassium hydroxide (KOH), methylene blue (MB, $C_{16}H_{18}ClN_3S$), sodium hydroxide (NaOH), hydrochloric acid (HCl), distilled water, 96° ethanol, LR obtained from the essential oil distillation workshop of the Institute of Life Sciences at Thai Nguyen University of Agriculture and Forestry. The equipment used for the preparation of biochar is a 100 mL hydrothermal reactor (TOB Reactor, China).

2.2. Synthesis and Material Characteristics

Material Synthesis:

The process involved preparing the LR by drying and finely grinding it before placing it into a covered porcelain crucible and wrapping

it in aluminum foil. Subsequently, it underwent pyrolysis at 500 °C for 1 hour. Afterward, it was allowed to naturally cool to room temperature and finely ground to produce B500 material. A portion of B500 was dispersed in a 5M KOH solution in an ultrasonic bath at 70-80 °C for 3 hours. Following this, it was thoroughly washed with distilled water until reaching a neutral pH, dried, and finely ground again to yield B5KOH material. Storage of the materials was carried out in sealed plastic bags within a desiccator when not in use.

Material Characterization:

The bonding characteristics and functional groups of the materials underwent analysis using an IR Spectrum Two spectrometer by Perkin Elmer (USA) within the wavenumber range of 4000 – 400 cm^{-1} at the Laboratory Center of the University of Science, Thai Nguyen University. Elemental composition analysis was conducted via energy-dispersive X-ray spectroscopy (EDS) on a Jeol 6490 – JED 2300, while material morphology examination was performed using scanning electron microscopy (SEM) on a Hitachi S-4800 (Japan) at the Institute of Materials Science, Vietnam Academy of Science and Technology. Determination of the porous structure and specific surface area was achieved using the Brunauer-Emmett-Teller (BET) method on a TriStar 3000 V6.07 at the Faculty of Chemistry, Hanoi National University of Education. The point of zero charge was experimentally determined using the pH drift method with a NaCl solution: Prepare 0.1 M NaCl solutions with an initial pH ranging from 2.0 to 11.0 (adjusted using 0.1 M HCl or 0.1 M NaOH solution); add to each 10 mL of NaCl solution 0,01 g of B5KOH, mix until completely dispersed; after 48 hours, the final pH was measured, and the zero point of charge was determined from the plot of ΔpH versus initial pH, where ΔpH = final pH - initial pH = 0.

2.3. Adsorption Experiment

MB was investigated for their adsorption behavior using B500 and B5KOH samples at different pH for 3 hours. Notably, B5KOH demonstrated a significantly higher adsorption capacity for MB. Subsequent investigations aimed to assess the adsorption of MB onto B5KOH across a range of concentrations from 5 to 500 mg/L, utilizing B5KOH dose varying from 1.0 g/L to 10.0 g/L time intervals spanning 5 to 900 minutes at both 25 °C and 40 °C. Each experimental trial involved the preparation of an MB solution with a specific concentration, precise pH adjustment, aliquoting 10 mL into a 15 mL Falcol tube, addition of a predetermined amount of B5KOH, agitation of the mixture for the specified duration, centrifugation at 5000 rpm for 15 minutes, filtration and extraction of the solution, and determined the concentration of the MB before and after adsorption using UV-Vis spectroscopy at wavelengths of 664, with standard curves established within the concentration range of 0.1 to 20 mg/L. Control samples underwent identical treatment procedures but lacked MB addition. Each experiment was replicated three times to obtain the mean value.

The MB adsorption efficiency (AE, %) and the adsorption capacity (q_t, mg/g) of the material are calculated using the following formulas:

$$AE = \frac{C_o - C_t}{C_o} x100\% (\%) \quad (1)$$

$$q_t = \frac{C_o - C_t}{m} V \quad (mg/g) \quad (2)$$

Where: C_o and C_t are the concentrations of MB in the solution before and after the adsorption time t (minutes); m is the mass of the adsorbent material (g); V is the volume of the working solution (L).

Material reusability:

The material, after adsorbing MB, is collected, washed with alcohol and distilled water, and then immersed in 1 M HCl, changing the solvent every 3-5 hours. After 24 hours, it is rinsed again with absolute alcohol three times, then washed with distilled water until neutral [21]. Finally, it is dried at 70 - 80 °C for reuse.

3. Results and Discussion

3.1. Material Characteristics

Figure 1a shows the EDS patterns of LR and pyrochar samples, the elemental composition of samples is shown in Table 1. LR contains high carbon content, 62.12%, making it is a potential feedstock to produce carbon-rich biochar. After pyrolysis, the carbon content in the B500 sample increased to 82.33%. This is due to the effect of heat during calcination, which broke the C–O bond, leading to the release of oxygen-containing compounds from LR and enhancing the carbonization process. The carbon content of the B5KOH sample further increased to 87.99% following KOH activation. This increase is due to KOH and ultrasonic vibration at 80-90 ^{o}C, which continued to oxidize B500, releasing oxygen-containing gases, or dissolved salts, encouraging pore formation. It also removed tar and other impurities in the pyrochar, such as SiO_2. As a result, the oxygen content continued to decrease, the carbon content continued to increase and the pore size also increased. This change was confirmed by the BET analysis results. This elevated carbon content surpasses that reported in comparable biochar studies involving materials such as rice straw [22] and corn stalk [23]. Furthermore, trace amounts of elements including K, Na, Ca, Cl, Si, etc., persist in the samples, constituting mineral components naturally present in the original LR's chemical composition, occurring in both inorganic and organometallic forms, thereby augmenting the material's polar properties.

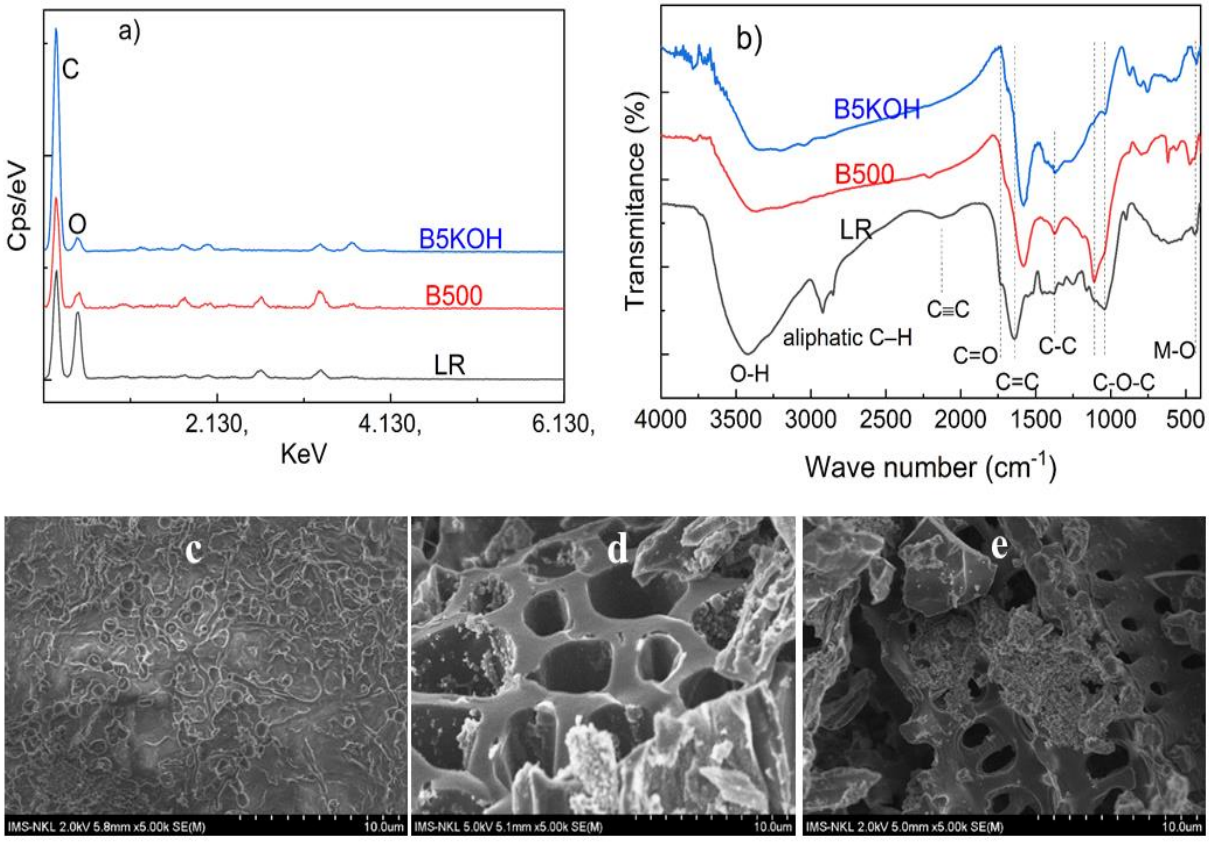

Figure 1. EDS spectrum (a), IR spectrum (b)SEM images of LR (c), B500 (d), and B5KOH (e) samples.

Table 1. Elemental composition and Pore parameters of LR and pyrochar samples

sample	Elements (%)						Pore parameters		
	C	O	Si	P	K	Ca	BET (m^2/g)	V_{Pore} (cm^3/g)	d_{Pore} (nm)
LR	62.12	36.79	0.09	0.10	0.32	0.07	-	-	-
B500	82.44	15.10	0.20	0.20	0.24	0.41	32.66	0.010127	8.5
B5KOH	87.99	10.87	0.16	0.22	0.23	0.31	79.90	0.036393	19.8

Figure 1b shows that, upon the pyrolysis of LR, marked alterations in the sample's bonding structure were observed: i) Broad peaks in the 3400 cm^{-1} region, indicative of the stretching vibration of hydrogen-bonded hydroxyl groups (derived from carboxylic, phenolic, or alcoholic moieties) or adsorbed water molecules in the residue, reduced intensity and expanded; ii) Characteristic peaks corresponding to aliphatic C-H stretching (from aromatic methoxy groups, methyl, and methylene groups of side chains) and aromatic C-H stretching at wavenumbers of 2922 and 2844 cm^{-1}, respectively, were scarcely discernible in the biochar; iii) Peaks at 1737 and 1640 cm^{-1} in the LR shifted to 1696 and 1582 cm^{-1}, respectively, indicative of C=O bonds in carbonyl or carboxyl groups (representing C=O stretching vibrations of ketones, aldehydes, lactones, or carboxyl groups, and C=C vibrations in aromatic rings) [24]; iv) the characteristic peak at 1034 cm^{-1} corresponding to C-O-C bonds also shifted to 1104 cm^{-1}; and v) peak in the region of 2190 cm^{-1} to 2330 cm^{-1}, characteristic of C≡C bonds in the LR [25], exhibited significant reduction in sample B500 and were absent in sample B5KOH. Furthermore, distinct peaks at 470 and 617 cm^{-1} emerged in the pyrolyzed samples, typically associated with metal-oxygen bonds, potentially enhancing the adsorption process.

The SEM image of the LR powder (Figure 1c) shows that the LR surface is monolithic, with a peeling phenomenon and many thin, small scales. This is the result of the essential oil distillation process. After calcinating at 500 °C for 1 hour, the original structure of LR 1d) was disrupted, leading to the creation of voids (Figure 1d).

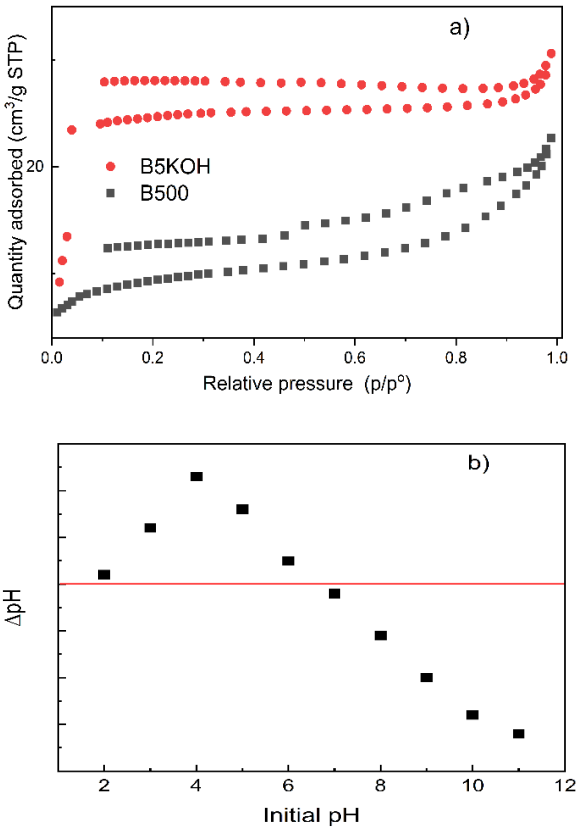

Figure 2. a) BET diagram and b) Isoelectric point of the B5KOH material

Some of these voids undergo fragmentation, resulting in the formation of small, porous fragments. When the B500 sample is treated

with potassium hydroxide at temperatures of 78-80 °C and exposed to ultrasonic vibration (Figure 1e), the fragments adhering to the walls of the porous voids detach, further disintegrating into minute and porous fragments. Consequently, the thermal decomposition of the material yields a porous void structure, while activation continues to excavate the small structural fragments, anticipating a sustained augmentation in a specific surface area. This phenomenon was corroborated through BET analysis (Figure 2a and Table 1).

Figure 2a shows the isotherms curves of B500 and B5KOH samples, where the shape of the H3-type hysteresis loop (according to IUPAC classifications), which represents the mesoporous structure with adsorbents is an aggregate of plate-like particles giving rise to slit-shaped pores [26]. Some pore parameters are shown in Table 1. The BET-specific surface area of B5KOH, compared to numerous studies involving other biomass sources, is not notably high, it exhibits a twofold increase compared to B500. Moreover, the pores of B5KOH are notably more expanded than those of B500. It is the result of the activation of B500 by KOH and ultrasonic vibration at 80-90 ^{o}C as analyzed above. Experimental determination of the isoelectric point of B5KOH (Figure 3b) indicates an isoelectric point of 6.8. Thus, when the material is in an environment with a pH > 6.8, the material surface becomes negatively charged, and vice versa.

3.2. Study of Dye Adsorption Capability

3.2.1. Factors Influencing Adsorption

The influence of some factors on the MB adsorption is depicted in Figure 3.

Figure 3a depicts a gradual increase in adsorption efficiency as the pH rises from 3 to 8, followed by a decline beyond pH 8. Due to the pH_{pzc} of B5KOH being 6.8, it means that a decrease in solution pH results in a heightened positive charge on the B5KOH surface, diminishing favorable cation adsorption and reducing efficiency. In addition, the lower the pH, the more mobile the H^+ ion, the stronger the adsorption competition with MB cation, the more electropositive the material surface, and the lower the adsorption efficiency of MB. Conversely, with increasing pH from 7, the surface exhibits augmented negative charge, rendering it conducive for adsorbing positively charged ions. However, at pH levels higher than 8, despite a larger negative surface charge, the adsorption efficiency slightly decreases. This result was similar to some other studies [27, 28]. At higher pH, structural alterations in MB may diminish adsorption capacity [29]. In addition, the higher the pH, the more OH^- ion, increased electrostatic interaction between OH^- ion and MB cation also reduces the positive charge of MB cation, which may contribute to reduced adsorption efficiency. At each pH, the MB adsorption efficiency of the B5KOH sample was higher than that of B500. This result was consistent with predictions drawn when analyzing material characteristics. Subsequent adsorption experiments will be conducted at pH 8 with a B5KOH sample.

Figures 3b and 3c reveal that as material concentration rises and the concentration of adsorbed MB decreases, adsorption efficiency increases. This phenomenon was explicable by the concurrent increase in material concentration and surface area, facilitating greater interaction opportunities. Conversely, if the surface area remains constant while the number of adsorbed molecules decreases, the likelihood of adsorbent-adsorbate interaction rises, reducing competitive adsorption factors and boosting efficiency.

Figure 3d illustrates the rapid onset of the adsorption process upon MB contact with lemongrass biochar. Adsorption efficiency surpasses 70% within the initial 5 minutes and gradually stabilizes after 30 minutes, with no significant efficiency increase observed even with extended contact up to 180 minutes.

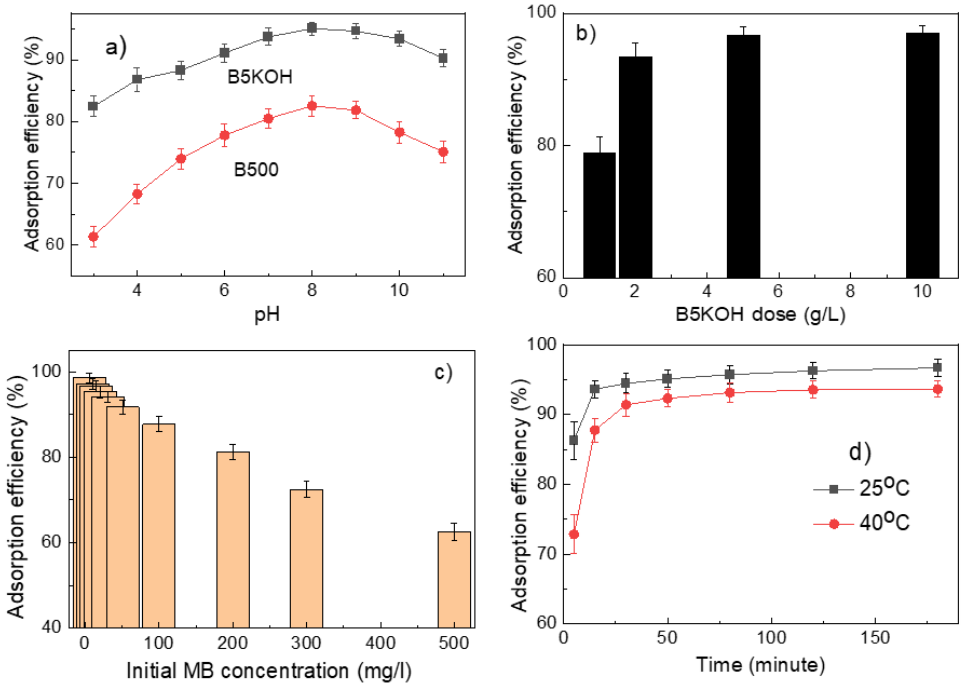

Figure 3. Factors affecting adsorption: a) The pH of the solution during the adsorption of 20 mg/L MB by 2 g/L B5KOH at 25 °C for 3 hours. b) The amount of B5KOH material involved in the adsorption of 15 mg/L MB at 25 °C for 3 hours at pH 8. c) The initial MB concentration adsorbed by 5 g/L B5KOH at 25 °C for 15 hours at pH 8.d) The temperature and time (adsorption of 15 mg/L MB by 5g/L B5KOH at 25 °C and 40 °C over time at pH 8).

B5KOH reusability is exemplified in Figure 4, where the adsorption efficiency of a 15 ppm MB solution by 5 g/L B5KOH exhibits negligible decline over four reuse cycles. Hence, the material not only facilitates facile recovery but also demonstrates highly efficient reuse.

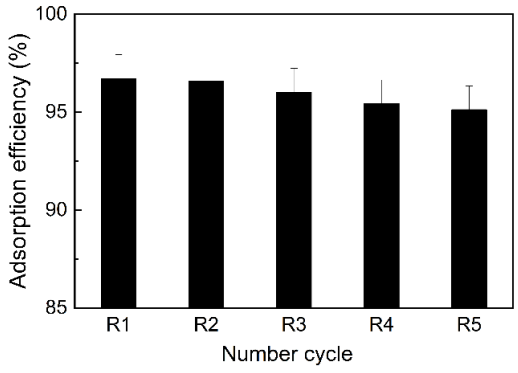

Figure 4. MB adsorption efficiency of B5KOH at adsorption/desorption cycles.

3.2.2. Adsorption Isotherms

Experimental data concerning the adsorption of MB at different concentrations using 5 g/L B5KOH were analyzed utilizing Langmuir, Freundlich, and Temkin isotherm adsorption models expressed in computational equations [30]:

$$q_e = q_m \frac{K_L C_e}{1 + K_L C_e} \quad (3)$$

$$q_e = K_F C_e^n \quad (4)$$

$$q_e = B\ln(K_T.C_e) \quad (5)$$

Here, q_e and q_m stand for the equilibrium adsorption capacity and the maximum monolayer adsorption capacity (mg/g), respectively. C_e represents the concentration of the adsorbed substance at equilibrium. K_L (L/mg), K_F (L/mg), and K_T (L/mg) denote the equilibrium constants as per the Langmuir, Freundlich, and Temkin isotherm models, respectively. The constant n in the Freundlich

equation reflects the homogeneity or heterogeneity of the adsorbent surface, with favorable adsorption occurring within the range of 0<n<1. B, a constant in the Temkin equation, is associated with the adsorption energy. The outcomes are depicted in Figure 5.

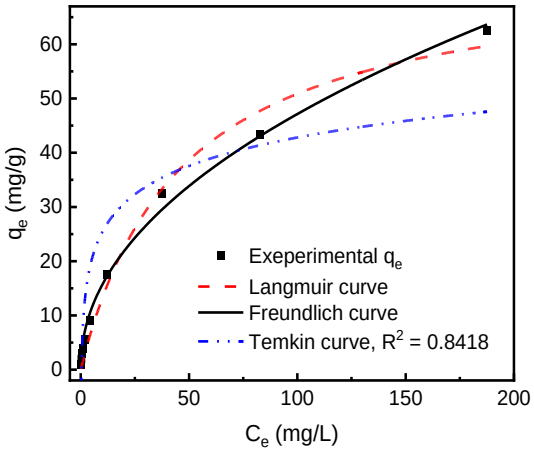

Figure 5. Adsorption isothermal equilibrium tendency of MB onto B5KOH.

Figure 5 reveals that the largest correlation coefficient R^2 is 0.9957, of the Freundlich model. This implies a closer alignment of the experimental data with the Freundlich model, with a Freundlich model parameter of n = 0.4777, conducive to favorable adsorption. This result allows us to conclude that the adsorbent material surface was homogeneous, permitting adsorption at all points across its surface. Predominantly, the interaction between the adsorbent and the adsorbate is physical, allowing for multilayer adsorption, with the initial layer serving as the adsorption site followed by condensation layers. The Freundlich equilibrium constant stands at 4.138 L/mg. Nonetheless, physical adsorption typically displays reduced stability and declines with rising temperatures. The Langmuir model's R^2 value, 0.9852, quite large, indicated a degree of congruence with this model, proving that the interaction between B5KOH and MB still included part of the chemical interaction. As per the Langmuir model, the maximum adsorption capacity (q_m) of the primary layer approximates 74.44 mg/g. This q_m value was smaller than some biochars derived from globe artichoke leaves [10] or lychee seed [13] but higher than LR [31] and some other biochars, such as Biochar Derived from *Mimosa Pigra* Plant [32], dragon fruit branches [33], waste nut shell-based hydrochar [34] or KOH activated bamboo biochar [35].

3.2.3. Adsorption Kinetics

Experimental data from the adsorption process of 15 mg/L MB by 5 g/L B5KOH at pH 8, conducted over time at both room temperature and 40 °C, was utilized to investigate the kinetics of the process through various kinetic models: diffusion kinetics, first-order reaction kinetics, and second-order reaction kinetics, represented by the following equations [30]:

$$q_t = k_d t^{0.5} + C \quad (6)$$

$$q_t = q_e\left(1 - e^{-k_1 t}\right) \quad (7)$$

$$q_t = \frac{k_2 q_e^2 t}{1 + k_2 q_e t} \quad (8)$$

Where: k_d (mg·g^{-1}·min$^{-0.5}$), k_1 (min^{-1}), and k_2 (g·mg^{-1}·min^{-1}) are the rate constants corresponding to the diffusion process, first-order reaction rate and second-order reaction rate, respectively; C is a parameter within the diffusion kinetics equation. The simulated results from these models are illustrated in Figure 6.

Figure 6 illustrates that the pseudo-second-order kinetic model demonstrates the highest correlation coefficient, whereas the diffusion kinetic model exhibits the lowest. Consequently, the interaction phase between the adsorbent and adsorbate progresses at a slower rate, following a pseudo-second-order reaction pattern, thereby resembling characteristics akin to chemical reactions.

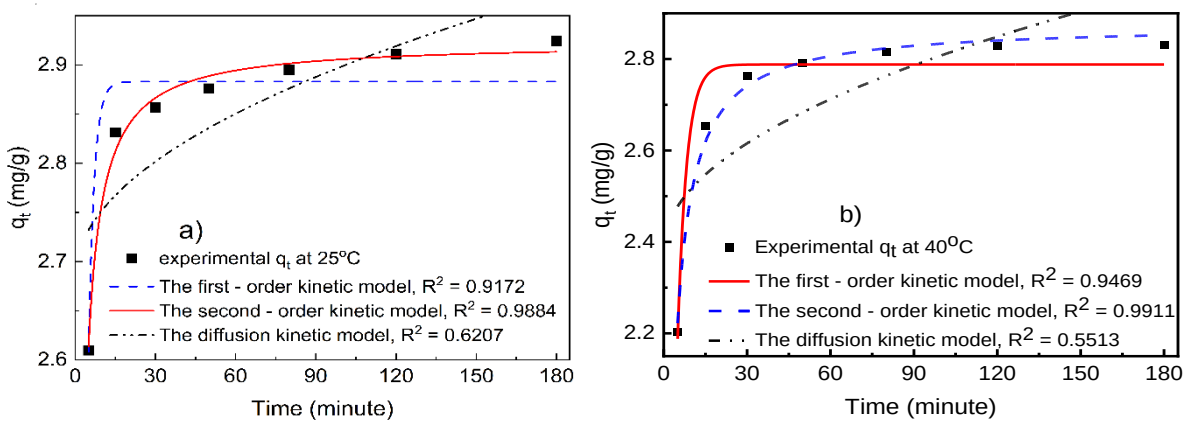

Figure 6. Adsorption kinetic models of MB onto B5KOH at 25 °C (a) and 40 °C (b).

3.2.4. Adsorption Thermodynamic

By employing outcomes from the Freundlich adsorption isotherm equation and the second-order kinetics equation, numerous thermodynamic parameters can be computed utilizing the subsequent equations [36, 37]:

$$K=\frac{C_{eA}}{C_e} \quad (9)$$

$$log\frac{K_{T_2}}{K_{T_1}} = \frac{\Delta H}{2.303R}.\left(\frac{1}{T_2}\frac{1}{T_1}\right) \quad (10)$$

$$\Delta G=-RTlnK \quad (11)$$

$$log\frac{k_{T_2}}{k_{T_1}} = \frac{E_a}{2.303R}.\left(\frac{1}{T_2}-\frac{1}{T_1}\right) \quad (12)$$

where R = 8.314 J/mol K), T (Kelvin) is the absolute temperature, and Ce (mg/L) is the equilibrium concentration of MB in the solution. C_{eA} (mg/L) is the concentration of Mb on the adsorbent at equilibrium, C_{eA} = C_o-C_e. K is the equilibrium constant, k is the adsorption rate constant, and E_a is the activation energy. The results are outlined in Table 2.

Table 2. Some thermodynamic parameters of the MB adsorption process by B5KOH

Parameters	25 °C	40 °C
Rate constant k_2 ((mg/g)$^{-1}$.min^{-1})	0.5783	0.2368
Activation energy E^* (kJ)	20.047 kJ	
Experimental q_e (mg/g)	2.9242	2.8317
Theoretical q_e (mg/g)	2.9229	2.8752
Equilibrium constant K	29.2421	14.7046
ΔG = -RTlnK (kJ/g.K)	-8.363	-6.995
ΔH (kJ)	-15,435	

Table 2 reveals the following: i) There is close agreement between the maximum experimental and theoretical adsorption capacities, implying consistency between theory and experiment; ii) The adsorption process demonstrates ΔG < 0, indicating spontaneity and a favorable energy direction, with the process being exothermic (ΔH < 0); notably, the process at 40 °C displays lower rate and equilibrium constants compared to that at 25 °C; and iii) Both ΔH and ΔG values suggest that physical interactions predominantly govern the process rather than chemical interactions.

Thus, according to the results of the influence of pH on adsorption efficiency, the suitability of the adsorption experiment followed the Freundlich model, the decrease in adsorption efficiency by increasing

temperature, the calculated ΔG and ΔH values, all show the adsorption mechanism was primarily driven by physical interactions. That was electrostatic between MB cation and the electronegative surface of the adsorbent, such as O in the O-H bond, C=O bond, electron-rich centers as C=C, aromantic ring,… etc.

4. Conclusion

Pyrochar derived from the lemongrass essential oil distillation residue, and subsequently activated with alkali displayed a notable increase in both specific surface area and carbon content compared to non-activated counterparts. The pyrolysis process conducted at 500 °C yielded a porous structure characterized by high porosity. Activation procedures contributed to the cleansing of surfaces, fragmentation, and a substantial augmentation in the porosity of minute material clusters. This material exhibited remarkable adsorption efficiency for MB at pH 8, achieving adsorption equilibrium within a brief timeframe, typically ranging from 30 to 50 minutes, across MB concentrations spanning from 5 to 500 mg/L, employing material concentrations of 1-10 g/L. The adsorption process adhered to the Freundlich isotherm model and proceeded via second-order kinetic mechanisms. Furthermore, the adsorption process was spontaneous, with physical interactions primarily driving the interaction between the material and MB.

Acknowledgements

We are gratefully acknowledged for the support from Thai Nguyen University of Science.

References

[1] A. K. Behera, K. P. Shadangi, P. K. Sarangi, Effcient Removal of Rhodamine B Dye using Biochar as an Adsorbent: Study the Performance, Kinetics, Thermodynamics, Adsorption Isotherms and its Reusability, Chemosphere, Vol. 354, 2024, pp. e141702, https://doi.org/10.1016/j.chemosphere.2024.141702.

[2] P. O. Oladoye, T. O. Ajiboye, E. O. Omotola, O. J. Oyewola, Methylene Blue Dye: Toxicity and Potential Elimination Technology from Wastewater, Results in Engineering, Vol. 16, 2022, pp. e100678, https://doi.org/10.1016/j.rineng.2022.100678.

[3] M. M. Mabel, T. R. Sundararaman, N. Parthasarathy, J. Rajkumar, Chitin Beads from Peneaus sp. Shells as a Biosorbent for Methylene Blue Dye Removal, Pol. J. Environ. Stud, Vol. 28, No. 4, 2019, pp. 2253-2259, https://doi.org/10.15244/pjoes/90359.

[4] A. K. Moorthy, B. G. Rathi, S. P. Shukla, K. Kumar, V. S. Bharti, Acute Toxicity of Textile Dye Methylene Blue on Growth and Metabolism of Selected Freshwater Microalgae, Environ, Toxicol. Pharmacol., Vol. 82, 2021, pp. e103552, https://doi.org/10.1016/j.etap.2020.103552.

[5] S. M. Peneyra, K. Lerpiriyapong, E. R. Riedel, N. S. Lipman, C. Lieggi, Impact of Pronase, Sodium Thiosulfate, and Methylene Blue Combinations on Development and Survival of Sodium Hypochlorite Surface-Disinfected Zebrafish (*Danio rerio*) Embryos, Zebrafish, Vol. 17, No. 5, 2020, pp. 342-353, https://doi.org/10.1089/zeb.2020.1917.

[6] A. M. McDonnell, I. Rybak, M. Wadleigh, D. C. Fisher, Suspected Serotonin Syndrome in a Patient Being Treated with Methylene Blue for if Osfamide Encephalopathy, J. Oncol. Pharm. Pract., Vol. 18, No. 4, 2012, pp. 436-439, https://doi.org/ 10.1177/1078155211433231.

[7] R. R. Ramsay, C. Dunford, C. K. Gillman, Methylene Blue and Serotonin Toxicity: Inhibition of Monoamine Oxidase A (MAO A) Confirms a Theoretical Prediction, Br. J. Pharmacol., Vol. 152, No. 6, 2007, pp. 946-951, https://doi.org/10.1038/sj.bjp.0707430.

[8] E. Santoso, R. Ediati, Y. Kusumawati, H. Bahruji, D. O. Sulistiono, D. Prasetyoko, Review on Recent Advances of Carbon Based Adsorbent for Methylene Blue Removal from Waste Water, Materials Today Chemistry, Vol. 16, 2020, pp. e100233, https://doi.org/10.1016/j.mtchem.2019.100233.

[9] Z. Liu, Z. Wang, H. Chen, T. Cai, Z. Liu, Hydrochar and Pyrochar for Sorption of Pollutants in Wastewater and Exhaust Gas: A Critical Review, Environmental Pollution, Vol. 268, 2021, pp. e115910, https://doi.org/10.1016/j.envpol.2020.115910.

[10] M. Benadjemia, L. Milière, L. Reinert, N. Benderdouche, L. Duclaux, Preparation, Characterization and Methylene Blue Adsorption of

Phosphoric Acid Activated Carbons from Globe Artichoke Leaves, Fuel Process, Technol., Vol. 92, No. 6, 2011, pp. 1203-1212, https://doi.org/10.1016/j.fuproc.2011.01.014.

[11] M. A. Islam, M. J. Ahmed, W. A. Khandav, M. Asif, B. H. Hameed, Mesoporous Activated Coconut Shell-Derived Hydrochar Prepared via Hydrothermal Carbonization-NaOH Activation for Methylene Blue Adsorption, J. Environ. Manag., Vol. 203, Part 1, 2017, pp. 237-244, https://doi.org/10.1016/j.jenvman.2017.07.029.

[12] V. Tharaneedhar, P. S. Kumar, A. Anbalagan, C. Ravikumar, J. Vasudevan, Prediction and Interpretation of Adsorption Parameters for the Sequestration of Methylene Blue Dye from Aqueous Solution using Microwave Assisted Corncob Activated Carbon, Sustain, Mater, Technol., Vol. 11, 2017, pp. 1-11, https://doi.org/ 10.1016/j.susmat.2016.11.001.

[13] S. Sahu, S. Pahi, S. Tripathy, K. Singh, A. Behera, U. K. Sahu, R. K. Patel, Adsorption of Methylene Blue on Chemically Modified Lychee Seed Biochar: Dynamic, Equilibrium, and Thermodynamic Study, Journal of Molecular Liquids, Vol. 315, 2020, pp. e113743, https://doi.org/10.1016/j.molliq.2020.113743.

[14] A. Subratti, J. L. Vidal, L. J. Lalgee, F. M. Kertonb, N. K. Jalsa, Preparation and Characterization of Biochar Derived from the Fruit Seed of Cedrela Odorata L and Evaluation of Its Adsorption Capacity with Methylene Blue, Sustainable Chemistry and Pharmacy, Vol. 21, 2021, pp. e100421, https://doi.org/10.1016/j.scp.2021.100421.

[15] K. Tohdee, S. Semmad, A. Jotisankasa, B. Jongsomj it, T. Somsiripan, Asadullah, Sustainable Adsorption of Methylene Blue onto Biochar-based Adsorbents Derived from Oil Palm Empty Fruit Branch: Performance and Reusability Analysis, Bioresource Technology Reports, Vol. 25, 2024, pp. e101755, https://doi.org/10.1016/j.biteb.2023.101755.

[16] E. A. Azim, M. Samy, M. Hanafy, H. Mahanna, Novel Mint-stalks Derived Biochar for the Adsorption of Methylene Blue Dye: Effect of Operating Parameters, Adsorption Mechanism, Kinetics, Isotherms, and Thermodynamics, Journal of Environmental Management, Vol. 357, 2024, pp. e120738, https://doi.org/10.1016/j.jenvman.2024.120738.

[17] S. Sen, M. Israr, S. Singh, M. K. Singh, R. S. Verma, D. U. Bawankule, Pharmaceutical, Cosmeceutical, Food Additive and Agricultural Perspectives of Cymbopogon Martini: A Potential Industrial Aromatic Crop, South African Journal of Botany, Vol. 158, 2023, pp. 277-291, https://doi.org/10.1016/j.sajb.2023.05.007.

[18] M. Greenway, P. de Rozari, A. El Hanandeh, Plant Growth and Nutrient Accumulation in Melaleuca Quinquenervia and Cymbopogon Citratus Treating High Strength Sewage Effluent in Constructed Wetland Systems with Biochar Media, Ecological Engineering, Vol. 180, 2022, pp. e106667, https://doi.org/10.1016/j.ecoleng.2022.106667.

[19] K. A. A. Putri, A. Keereerak, W. Chinpa, Novel Cellulose-Based Biosorbent from Lemongrass Leaf Combined with Cellulose Acetate for Adsorption of Crystal Violet, International Journal of Biological Macromolecules, Vol. 156, 2020, pp. 762-772, https://doi.org/10.1016/j.ijbiomac.2020.04.100.

[20] P. Kumari, W. Raza, A. Meena, Lemongrass Cellulose Nanofibers for Controlled Release of Curcumin and Its Mechanism of Action, Industrial Crops and Products, Vol. 173, 2021, pp. e114099, https://doi.org/ 10.1016/j.indcrop.2021.114099.

[21] Y. S. Ngoh, M. A. Nawi, Role of Bentonite Adsorbent Sub-layer in the Photocatalytic Adsorptive Removal of Methylene Blue by the Immobilized TiO_2/Bentonite System, Int. J. Environ. Sci. Technol., Vol. 13, 2016, pp. 907-926, https://doi.org/10.1007/s13762-015-0928-5.

[22] L. Wei, J. Lu, Adsorption of Microcystin-LR by Rice Straw Biochars with Different Pyrolysis Temperatures, Environmental Technology and Innovation, Vol. 23, 2021, pp. e101609, https://doi.org/ 10.1016/j.eti.2021.101609.

[23] R. Xie, Y. Zhu, H. Zhang, P. Zhang, L. Han, Effects and Mechanism of Pyrolysis Temperature on Physicochemical Properties of Corn Stalk Pellet Biochar based on Combined Characterization Approach of Microcomputed Tomography and Chemical Analysis, Bioresource Technology, Vol. 329, 2021, pp. e124907, https://doi.org/ 10.1016/j.biortech.2021.124907.

[24] M. E. Mahmoud, S. A. A. A. Ali, S. M. T. Elweshahy, Efficient and Ultrafast Removal of Cd(II) and Sm(III) from Water by Leaves of Cynara Scolymus Derived Biochar, Materials Research Bulletin, Vol. 141, 2021, pp. e111334, https://doi.org/10.1016/j.materresbull.2021.111334.

[25] F. M. Adesemuyi, M. A. Adebayo, A. O. Akinola, E. F. Olasehinde, K. A. Adewole, L. Lajide, Preparation and Characterisation of Biochars from Elephant Grass and their Utilisation for Aqueous Nitrate Removal: Effect of Pyrolysis Temperature,

Journal of Environmental Chemical Engineering, Vol. 8, No. 6, 2020, pp. e104507, https://doi.org/10.1016/j.jece.2020.104507.

[26] D. K. Mishra, S. K. Samad, A. K. Varma, V. A. Mendhe, Pore Geometrical Complexity and Fractal Facets of Permian Shales and Coals from Auranga Basin, Jharkhand, India, Journal of Natural Gas Science and Engineering, Vol. 52, 2018, pp 25-43, https://doi.org/10.1016/j.jngse.2018.01.014.S.

[27] K. Ghosh, A. Bandyopadhyay, Adsorption of Methylene Blue onto Citric Acid Treated Carbonized Bamboo Leaves Powder: Equilibrium, Kinetics, Thermodynamics Analyses. J. Mol. Liq., Vol. 248, 2017, pp. 413-424, https://doi.org/10.1016/j.molliq.2017.10.086.

[28] A. H. Jawad, M. A. M. Ishak, A. M. Farhan, K. Ismail, Response Surface Methodology Approach for Optimization of Color Removal and COD Reduction of Methylene Blue using Microwave-Induced NaOH Activated Carbon from Biomass Waste, Desalination Water Treat, Vol. 62, 2017, pp. 208-220, https://doi.org/10.5004/dwt.2017.20132.

[29] C. Djama, A. Bouguettoucha, D. Chebli, A. Amrane, H. Tahraoui, J. Zhang, L. Mouni, Experimental and Theoretical Study of Methylene Blue Adsorption on a New Raw Material, *Cynarascolymus* - A Statistical Physics Assessment, Sustainability, Vol. 15, No. 13, 2023, pp. e10364, https://doi.org/10.3390/su151310364.

[30] A. I. Adeogun, O. A. Osideko, M. A. Idowu, V. Shappur, O. A. Akinloye, B. R. Babu, Chitosan Supported $CoFe_2O_4$ for the Removal of Anthraquinone Dyes: Kinetics, Equilibrium and Thermodynamics Studies, SN Appl. Sci., Vol. 2, 2020, pp. e795, https://doi.org/10.1007/s42452-020-2552-3.

[31] V. T. Vi, Adsorption of Methylene Blue on Wastes from Lemongrass Leaves after Essential Oil Extraction, Journal of Science Technology and Food, Vol. 22, No. 2, 2022, pp. 3-10.

[32] N. X. Cuong, Study on Adsorption of Methylene Blue from Aqueous Solution by Biochar Derived from *Mimosa Pigra* Plant, VNU Journal of Science: Earth and Environmental Sciences, Vol. 37, No. 2, 2021, pp. 43-54, https://doi.org/10.25073/2588-1094/vnuees.4582.

[33] D. H. Sam, T. T. Suong, N. T. Hiep, T. A. Khoa, T. P. Vu, Adsorption of Methylene Blue onto Biochar Derived from the Dragon Fruit Branches, Can Tho University Journal of Science, Vol. 59, No. 5A, 2023, pp. 72-78, https://doi.org/10.22144/ctujos.2023.195.

[34] I. Tegin, M. F. Demirel, I. Alacabey, E. Yabalak, Investigation of the Effectiveness of Waste Nut Shell-based Hydrochars in Water Treatment: A Model Study for the Adsorption of Methylene Blue, Biomass Conversion and Biorefinery, Vol. 14, 2024. pp. 10399-10412, https://doi.org/10.1007/s13399-022-02996-y.

[35] Q. Ge, P. Li, M. Liu, G. Xiao, Z. Xiao, J. Mao, X. Gai, Removal of Methylene Blue by Porous Biochar Obtained by KOH Activation from Bamboo Biochar, Bioresources and Bioprocessing, Vol. 10, 2023, pp. e51, https://doi.org/10.1186/s40643-023-00671-2.

[36] J. H. Potgieter, C. Pardesi, S. Pearson, A Kinetic and Thermodynamic Investigation into the Removal of Methyl Orange from Wastewater Utilizing Fly Ash in Different Process Configurations, Environ, Geochem, Health, Vol. 43, 2021, pp. 2539-2550, https://doi.org/10.1007/s10653-020-00567-6.

[37] F. Zhang, X. Chen, F. Wu, Y. Ji, High Adsorption Capability and Selectivity of ZnO Nanoparticles for Dye Removal, Colloids Surfaces a Physicochem, Eng. Asp., Vol. 509, 2016, pp. 474-483, https://doi.org/10.1016/j.colsurfa.2016.09.059.